

FINAL REPORT

FFG Project number	870962	Recipient of the grant	Öbv-GmbH
Report No		reporting period	1.10.2018-30.09.2019
Report created by	Univ.Prof. Agathe Robisson, Michael Pauser		

Guide value for the size: 10-20 pages

1. Objectives and results

- Have the objectives underlying the grant agreement been achieved?
Are these goals still current or realistic?
Attention: Changes to targets require FFG approval.
- Compare the objectives with the results achieved.
- Describe "Highlights" and problems encountered in achieving the goal.

Requirements coming from European regulation No 305/2011 present new challenges to the construction industry in terms of energy savings in buildings (thermal insulation of materials) and sustainability (use of natural resources and low carbon footprint cements, recyclability).

This project aims at developing fundamental knowledge to support the industry, focusing on four distinct topics: characterization of material interfaces (new concrete applied on old concrete for renovation and rehabilitation), design of cement mortar infiltration for the production of insulation materials and lower carbon footprint materials, design of low-density cement for thermal insulation, and durability on recycled concrete.

This first year marks significant achievements:

- Development of novel setups to make quantitative measurements: stereoscopic measurement of roughness, visualization of infiltration of cement and rheological protocols, foam mixing-ability and stability measurement.
- Selection of surfactants for foamability and film stability in solutions with increasing ionic calcium contents.
- Selection of tensile, shear and fracture tests for the quantification of interface strength. First results show superiority of the epoxy resin bonding.
- Year 1 detailed report was sent to all partners.

2. Work packages and milestones

2.1 overview tables

Explanation:

The tables are structured analogously to the grant application.

Basic date: date according to grant application or project plan valid according to contract

Current planning: Date according to the planning valid at the time of reporting.

Table 1: Work packages

AP No.	work package designation	Degree of completion	base date		Current		Achieved results / deviations
			start	end	start	end	
1	Project management		10.18	09.23	10.18	09.23	Launch meeting held 25.04.2019. Three intermediate meeting held with partners
2	State of the art	60%	10.18	09.19	10.18	09.20	Examination of EU legislation for recyclability in construction, foam cement, durability of recycled aggregate concrete.
3	Development of rheological tests and procedures	30%	10.18	09.21	10.18	09.21	Global and local (Ultrasonic Speckle Velocimetry, USV) rheological measurements are made to study mortars sedimentation, particle migration and slippage. Protocol to measure yield stress established.
4	Investigation of the influence of the mixing process	20%	10.18	09.21	10.18	09.21	Three additional laboratory mixers were acquired. Mixing protocols were established for each. More effort was spent on Task 7 to better define the problem at stake.
5	Influence of cement grain size distribution on concrete rheology foamability and setting properties	30%	10.18	09.20	10.18	09.20	Influence of surfactant chemistry was characterized in ionic calcium solutions.
6	Interfaces between old material and new concrete	20%	10.18	09.23	10.18	09.23	Stereoscopic method to quantify roughness was assembled and assessed. Results were compared with "Sandfleckmethode". Samples were prepared with cement bond and epoxy bond and mechanically characterized, under tensile and shear stress.
7	Device for measuring infiltration	30%	10.19	10.22	10.19	10.22	Although it was originally planned in the second year of research, this work package has already begun. Setups were built to mimic the porous bitumen infiltration for semi-rigid coatings. Mortars infiltration is tracked by a rapid camera. Temperature was studied through spread tests on flat bitumen.
8	Equipment for the production of cement foams	10%	10.19	10.23	10.19	10.23	Although it was originally planned in the second year of research, this work package has already begun. High shear mixing was used to study foamability. In-line mixers are being investigated.
9	Device for characterizing volume changes or limiting pressure of RA concretes	0%	10.19	10.23	10.19	10.23	This work package starts in the second year of research
10	High thermal insulation in a double walled tower	0%	10.22	10.23	10.22	10.23	This work package starts in the second year of research

Table 2: Milestones

No milestones have been defined in the project.

2.2 Description of the work carried out during the reporting period

- Describe the work carried out in the reporting period, structured according to work packages.
- Could the work steps and packages be worked out according to plan?
Were there significant deviations?
- The description also includes a possible change in the methodology applied.
Note: Changes in methodology and significant changes in the work plan.
require a permit from the FFG.

WP 1: Project management

Launch meeting happened 25.04.2019. Intermediate meetings were held with PORR, ASFINAG and VÖZ/Lafarge.

WP 2: State of the art

Information were obtained on EU legislation for recyclability in construction and presented on 25.04.2019.

Published results made on mortar rheology, foam cement and durability of recycled aggregate concrete (RAC) were examined. These are within basis for the rest of the work and listed there.

Recycled Aggregate Concrete

Recycling discarded concrete as new concrete aggregate has been proven to be a commercial and effective way for the sustainable development. When demolished concrete is crushed, a certain amount of mortar and cement paste from the original concrete remains attached to stone particles in the recycled aggregate (RA). The presence of adhered mortar on the surface of crushed concrete aggregate generally degrades the quality of the recycled aggregate and consequently the fresh and hardened properties of concrete made from it.

The internal defects and the adhesive mortar on the surface of RA cause the physical and mechanical properties of recycled aggregate concrete to deteriorate. Compared with the performance of natural aggregate concrete (NAC), the shrinkage and the water sorptivity of RA concrete (RAC) increased, but the strength, the elastic modulus and the durability decreased, which limits the application of RAC in structural concrete ([9], [1], [3]).

The replacement of natural aggregate (NA) with RCA can be total (100%) or partial (< 100%). However, the use of fine RCA below 2 mm is uncommon in recycled aggregate concrete because of the high water demand of the fine material smaller than 150 µm, which lowers the strength and increases the concrete shrinkage significantly. This high water absorption and high cohesion of fine RCA also makes concrete quality control very difficult.

Compared to natural aggregates, recycled concrete aggregates have:

- up to 10% lower density
- higher porosity and higher water absorption: for coarse RCA it ranges from 2% to 9% and for fine RCA from 5.5% to 13%,
- increased Los Angeles abrasion loss up to 70%.

The main difficulties in use of RCA are in its high water absorption rate which in turn significantly affects the workability of the RAC mix. At higher levels of coarse aggregate replacement, the water demand of the RAC will increase for a given workability and either a small increase in cement content may be necessary, or alternatively the use of water-reducing admixtures to maintain target strength requirements. The increase in water demand will depend on the RCA properties, i.e. its absorption.

Based on the comparative analysis of the latest experimental research (103 studies during last ten years) on the use of RCA in structural concrete (Pryce-Jenkins, 2011) it could be concluded that:

- the compressive strength is typically lower by 5–20%; commonly there is little effect below 30% replacement,
- the tensile strength is typically lower by 0–30%; commonly there is little effect below 50% replacement,
- the modulus of elasticity is typically reduced by 15–30%, although limit values reported are 5% and

45%; commonly there is little effect below 20% replacement,

- increased shrinkage typically by 10–20%,
- increased creep by 25–50%,
- increased water absorption typically by 40–50%,
- no effect on carbonation or even improved resistance of RAC compared to NAC,
- same or slightly decreased (up to 10%) freezing and thawing resistance,
- increased chloride penetration typically by 50–70%.

All results are given for RAC with 100% coarse aggregate replacement, compared to reference natural aggregate concrete. Properties of RAC with fine RCA are generally lower than properties of RAC with coarse RCA, especially absorption and shrinkage.

Durability of Recycled Aggregate Concrete

The published test data on durability-related properties of RAC are rather limited. Generally the properties of RAC are lower than the properties of corresponding NAC, mostly due to the lower quality of RCA. However, this reduction is not so high as to prevent RCA from being used as aggregate in low-to-medium strength structural concrete.

During their service life, concrete structures are always subjected to various types of loads and aggressive environments, so it is essential to evaluate the transport properties of RAC under a simultaneous application of stress. Several experimental studies on the water and chloride permeability of stressed normal concrete have shown that the applied loads can promote the growth of microcracks and interconnectivity, which in turn results in an increase of permeability of structural concrete ([4], [5], [6], [7], [8]).

Thus in evaluation of the durability of RAC it is essential to understand the influences of combined mechanical and environmental loads on the durability. Basically the fundamental relationship between stress and permeability should be known. Otherwise, the design service life of concrete structures will be overestimated if this effect is not properly taken into account. However, very little is known about this issue.

Parameters influencing the durability

The deterioration of the cementitious matrix and consequently the materials durability is largely dependent on its pore size, volume and connectivity. These factors govern the amount of surface area that is prone to attack by deleterious chemical reactions ([1]). Generally the main goal in evaluation of the RCAs durability is to assess the materials porosity and permeability (under combined action of external stress and environmental loads) as well as to understand the main differences between these two parameters.

The porosity is an intrinsic material property (amount of void space as % of the total volume). The origin of pores in concrete is on the one side due to the fact that the volume after a reaction becomes smaller than the volume before reaction of different solid complexes of cement (silicates: C3S and C2S) i.e. 3.6% and 0.4%. On the other hand, water added to concrete is far in excess of that required for hydration of the cement present. The amount of water needed to hydrate of cement is only 18-20% by weight of cement whereas the water added in most cases varies from 44-50% (w/c ratio), because of proper workability. Thus the generated pores in the concrete are the result of changes in volume of the hydration products and the amount of water left behind and evaporate with time (Figure 1.).

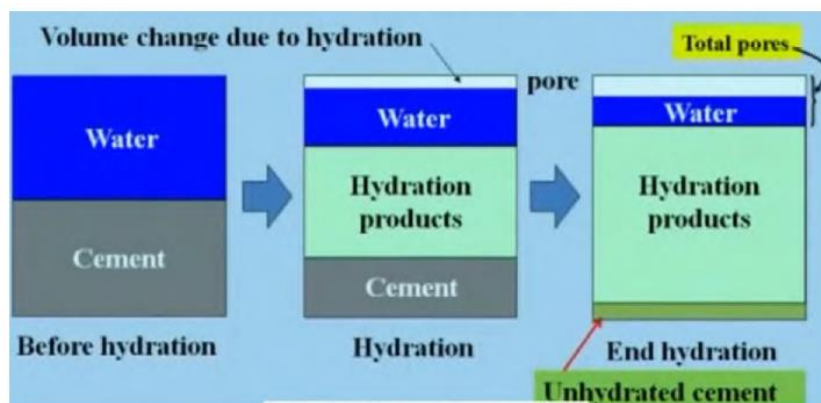


Figure 1. Volumetrics of cement hydration

Pores in concrete can be divided into five classes on basis of size: entrapped air (unintentional air in concrete), entrained air (intentional air through chemical admixtures), capillary pores (exist in cement paste and interfacial zone), gel pores (exist with the gel - hydration products), interlayer pores (exist in the gel). In concrete, most space is occupied by capillary pores.

Assessing the water absorption of concrete has been one of the most common approaches to indirectly evaluating the porosity of concrete and thus its potential durability. There is a consensus in the literature that as the replacement level of RA increases, so does the water absorption capacity of the resulting concrete (RAC), compared with the corresponding natural aggregate concrete (NAC).

The permeability in contrary is the ease (ability) with which something (fluids) can navigate (be transmitted) through the pores of the material. It depends upon:

- porosity (per se)
- interconnectivity of pores
- property of the navigating material (water, CO₂, chlorides)
- pressure of its application
- characteristics of the constituent materials (w/c, degree of hydration, degree of compaction, quality and, preconditioning temperature).

Porosity of RAC

Recycled concrete aggregates (RCAs) are expected to result in an increase in the water absorption of concrete, at a rate directly proportional to the RCA content. Figure

2 shows the relative sorptivity of RAC plotted against increasing coarse RCA content, with the interquartile region for mixes with 100% coarse RCA content (shaded area), where the sorptivity of RAC with increasing coarse RCA content is expected to progress. The sorptivity of RAC made with 100% coarse RCA is likely to be 31% to 56% higher than that of the control NAC.

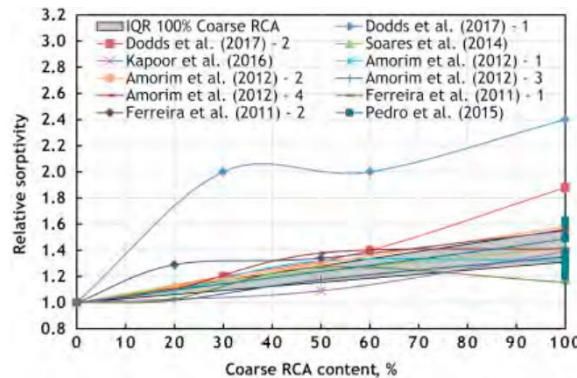


Figure 2. Relative sorptivity of recycled aggregate concrete with increasing coarse recycled concrete aggregate (RCA) content [1]

This increase occurs as a result of the increase in porosity of RCA due to the presence of old mortar adhered to the original NA, which results in a greater continuity of the porous structure. However, there is a greater probability of recycled masonry aggregates (RMAs) showing higher water absorption capacity compared with RCA and thus, for a given replacement level, the former is more likely to produce concrete exhibiting greater permeability and sorptivity than the latter. It was reported that water absorption by immersion and by capillary action of RAC with 100% coarse RMA may be in the region of 62% and 70%, respectively, higher than that of the control concrete.

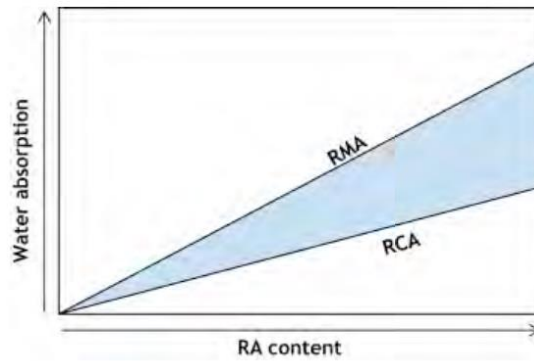


Figure 3. Overall behaviour of water absorption with increasing recycled aggregate (RA) content in the form of recycled masonry aggregate (RMA) and recycled concrete aggregate (RCA) [1]

Thus, the use of mixed recycled aggregates (MRAs) containing a higher proportion of RMA content is expected to result in concrete exhibiting higher water absorption than that made with MRAs having a higher proportion of RCA (Figure 3).

Depending on the age of the source concrete, the adhered mortar of the RCA obtained from it may still be hydrating, thereby helping RAC to develop a faster rate of porosity decrease with time compared with a corresponding NAC. In the study of Kou et al. (2011b), although the 28-day cumulative pore size distribution showed that RAC with

100% coarse RCA had higher porosity, after 5 years of water curing, RAC specimens showed a reduction in porosity of about 45%, whereas that of the control concrete was about 29%. This improvement of the RAC can be explained by the products of hydration of both the new and the old cement matrix, resulting in a reduction in the average pore size.

Permeability of RAC

The permeability of recycled aggregate concrete (RAC) gains special relevance because of the considerably higher water absorption of RA in comparison with natural aggregate (NA), which in turn reduces the durability of concrete. The permeation characteristics of RAC largely depend on the type of RA used.

Experimental studies also show that the permeability of common concrete often decreases with time due to the further hydration of concrete. For stressed concrete, there are more time-dependent factors, such as creep, microstructure and hydration. These factors influence the permeability of stressed concrete, but they are seldom discussed in the literature.

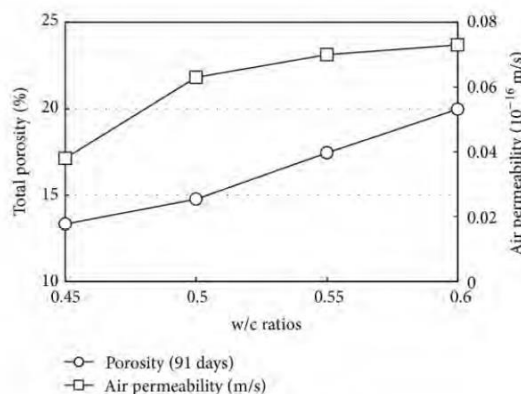


Figure 4. Porosity and permeability vs. w/c ratio [10]

Generally, both the porosity and (air) permeability increase with increasing w/c ratio (decreasing compression strength) ([10], [11], [12]) (Figs. 4. And 5.). Thus, permeability stays in direct correlation with the porosity, i.e. higher porosity results in higher permeability and vice versa. However, it is reported [12] that with increasing permeability and porosity a significantly weaker correlation is present, i.e. a much large scatter in results occur [12]. The reason for it is that permeability is not only dependent on total pore volume, but also other characteristics such as size distribution, shape, degree of connectivity and tortuosity of the pores. Another reason for the scatter is that differences in testing procedure (e.g. falling head vs. constant

head method) may also influence the results.

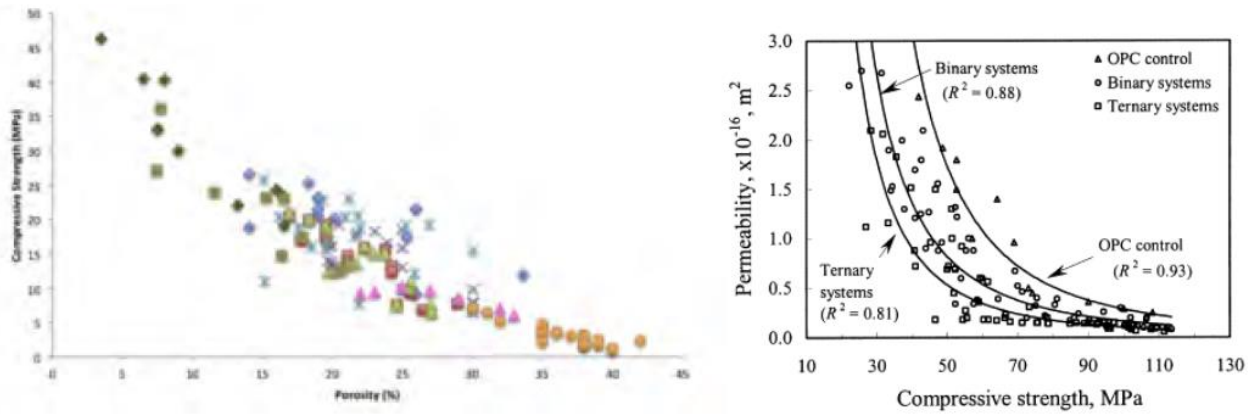


Figure 5. Porosity and permeability vs. compression strength [11], [12]

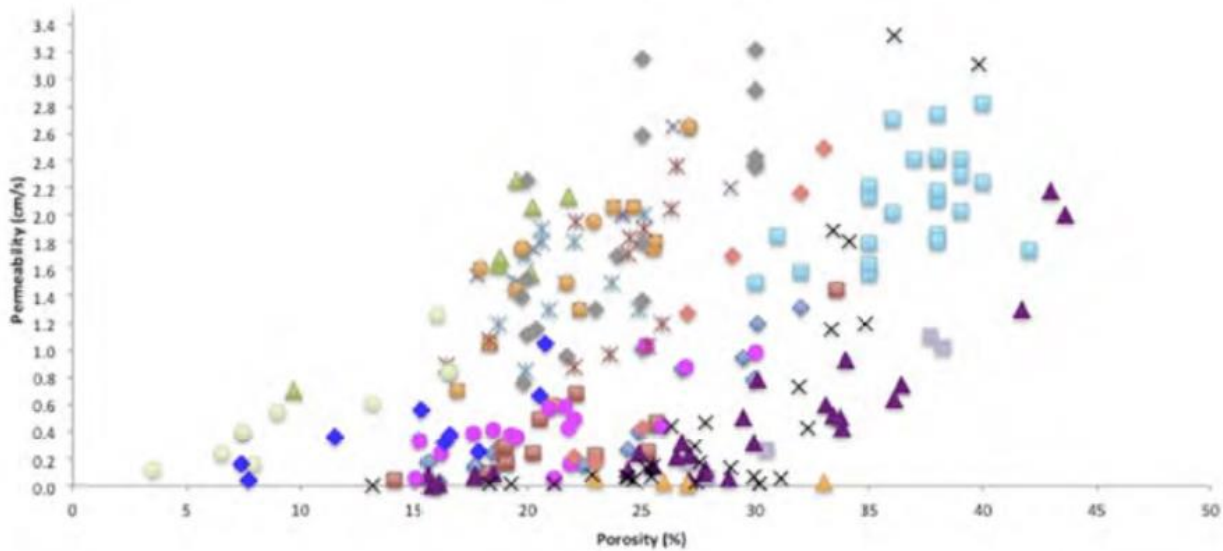


Figure 6. Permeability vs. porosity [12]

Even though the compression strength is related to w/c (and if w/c increases, total pore space increases, and therefore compression strength decreases). There are evidences that the amount of permeable pores varies lot at a given w/c (compression strength) or for the same permeable pores the compression strength range is fairly large. Thus in the performance (durability) based design permeability instead of compression strength should be considered as independent criteria for evaluating RAC.

References (selection)

- [1] Ravindra K.DhirOBEJorgede BritoRui V.SilvaChao QunLye, Recycled Aggregate Concrete: Durability Properties, Sustainable Construction Materials- Recycled Aggregates, Woodhead Publishing Series in Civil and Structural Engineering, 2019, Pages 365-418
- [2] S.B.MarinkovićM.Malešević.Ignjatović, Life cycle assessment (LCA) of concrete made using recycled concrete or natural aggregates, Eco-efficient Construction and Building Materials, Life Cycle Assessment (LCA), Eco-Labeling and Case Studies, 2014, Pages 239-266
- [3] New Trends in Eco-efficient and Recycled Concrete, Woodhead Publishing Series in Civil and Structural Engineering, 2019, Pages 329-356
- [4] Wang H.L., Lu C.H., Jin W.L., Bai Y. Effect of external loads on chloride transport in concrete. J. Mater. Civ. Eng. 2011;23:1043–1049. doi: 10.1061/(ASCE)MT.1943-5533.0000265.

- [5] Hoseini M., Bindiganavile V., Banthia N. The effect of mechanical stress on permeability of concrete: A review. *Cem. Concr. Compos.* 2009;31:213–220. doi: 10.1016/j.cemconcomp.2009.02.003.
- [6] Aldea C.M., Ghandehari M., Shah S.P., Karr A. Estimation of water flow through cracked concrete under load. *ACI Mater. J.* 2000;97:567–575.
- [7] Li H.M., Jin W., Song Y.J., Zhe W. Effect of external loads on chloride diffusion coefficient of concrete with fly ash and blast furnace slag. *J. Mater. Civ. Eng.* 2014;26:04014053:1–04014053:6.
- [8] Banthia N., Biparva A., Mindess S. Permeability of concrete under stress. *Cem. Concr. Res.* 2005;35:1651–1655.
- [9] Hailong Wang, Xiaoyan Sun, Junjie Wang, and Paulo J.M. Monteiro, Permeability of Concrete with Recycled Concrete Aggregate and Pozzolanic Materials under Stress, *Materials (Basel)*. 2016 Apr; 9(4): 252, doi: 10.3390/ma9040252
- [10] Kim et al. (2014) Effect of W/C Ratio on Durability and Porosity in Cement Mortar with Constant Cement Amount, *Advances in Materials Science and Engineering*
- [11] Khan and Lynsdale (2002), Strength, permeability, and carbonation of high- performance concrete, *Cement and Concrete Research*, Vol. 32
- [12] Alalea Kia, Hong S. Wong, Christopher R. Cheeseman, Clogging in permeable concrete: A review

WP 3: Development of rheological tests and procedures

Quick Facts

The focus of this work package is to define a reliable and systematic rheological procedure to characterize fresh concrete and mortar. Industrial standard laboratory methods (i.e. flow and spread tests) are compared with rheological measurements, where flows, stresses and strain rates are better controlled. Related to the Halbstarre Deckschichten application, a special setup composed by a mini-cone and a bitumen sheet is designed to study the mortar placement on real asphalt and to understand the influence of temperature and time.

To evaluate the reliability of conventional rheological protocols, we used an innovative and unique technique called Ultrasonic Speckle Velocimetry (USV). Preliminary tests were done at the ENS Lyon, and the eligibility of this technique was for the first time established for cement-based suspensions. In particular, we have shown how these measurements can avoid erroneous conclusions on the rheology of a mortar, due to wall slip and heterogeneous velocity fields throughout the sample.

Fresh paste characterization

Rheological measurements are also made to characterise the properties of our “model” fresh mortars and to compare them with the ones of an industrial product. Fresh material properties play a key role in the mortar placement and consequently in the durability of the final product. For this reason, studies on fresh mortar are made with both standard laboratory methods and rheological measurements, as sketched in fig. 6.

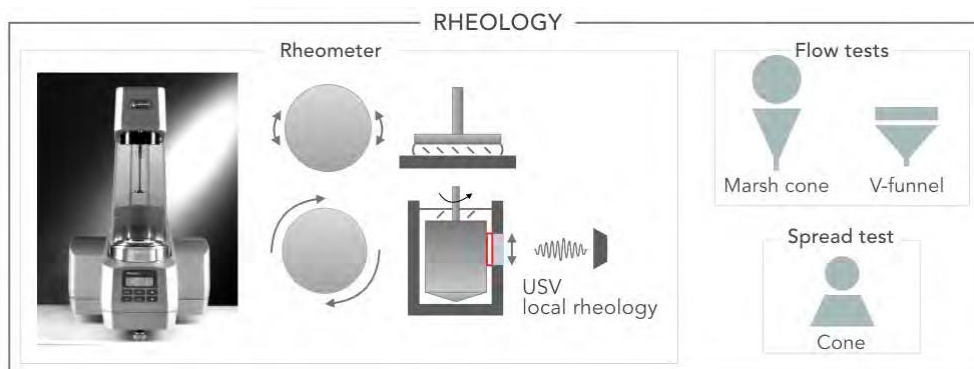


Figure 6: Rheological study of fresh mortar.

In particular, on the left part of fig. 6, there is a rheometer in oscillation (plate-plate geometry) and rotation (Couette geometry) modes; on the right part instead there are sketches of laboratory tools (flow and spread tests). With these rheological methods, we can have information about the elasticity and flow of the slurries and their (time) evolution. Moreover, an innovative and unique technique called Ultrasonic Speckle

Velocimetry USV (ENS Lyon, Prof. S. Manneville) is coupled with rheometry to follow at the same time the velocity profile and the local rheology of the slurries. Phenomena as migration, segregation, sedimentation under shear can therefore be detected.

0.4.1 Global rheology: minicone spread on bitumen sheet

We started our investigation on the properties of fresh mortar with the setup shown in fig. 7. A minicone is used to measure the slurry spread directly on a bitumen (flat) sheet. With this specific setup we want to mimic the

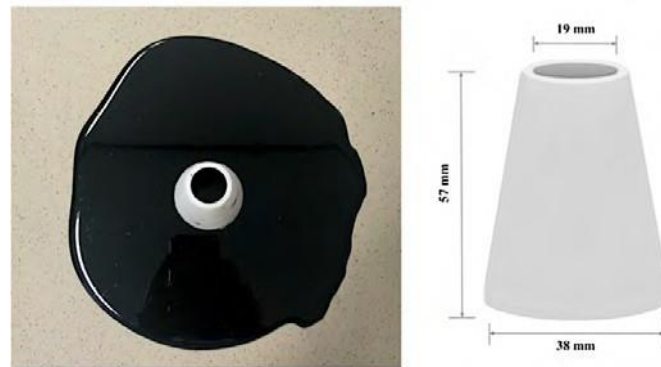


Figure 7: Minicone-bitumen setup: minislump test made on a bitumen sheet. The (inner) dimensions of the minicone (19,57 and 38 mm) are shown in the schematic diagram on the left.

mortar placement on the asphalt for semi-flexible coatings. In particular, we studied the influence of time on the slurry spread, and of the temperature on both the bitumen sheet and the mortar. As first, we compared in time our more stable (i.e. no bleeding) mortar (w/c 0.4, 0.3% bwoc of ACE 430) with the industrial product already mentioned.

In fig. 8 are shown the images of the final mini-cone spreads for both our mortar (a) and the industrial product (b).

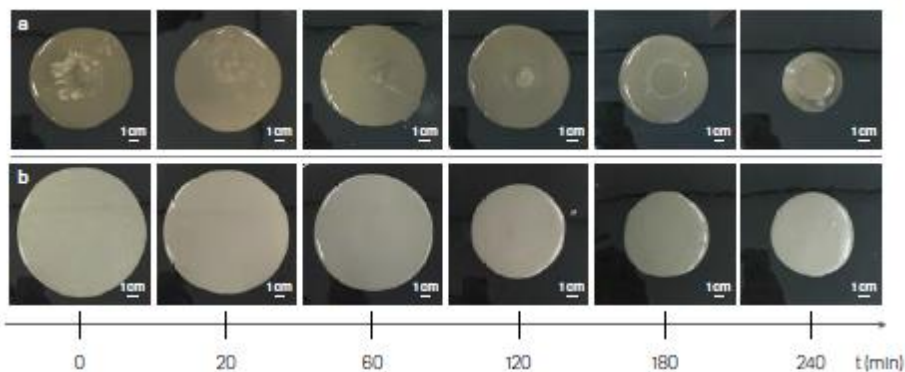


Figure 8: Time evolution of the minicone spread on bitumen sheet for (a) the mortar (w/c 0.4, 0.3% bwoc of ACE 430) and (b) one industrial product. All samples and bitumen sheets are at room temperature.

The spread diameter of the fresh mortar is around 11 cm and it is stable for the first 2 h. The industrial product instead has a 14 cm spread diameter, already reduced after the first hour. For both samples shown in fig. 8, the temperature is not altered (c.a. 25°C).

These tests suggest that the industrial product has a global higher spread compared to our mortar, probably due to the sand content 8 (which is not present in our mortar). Despite this, the sand is difficult to disperse without an high mixing and tends to sediment under shear. Figure 9 shows a slurry sample after a plate-plate rheology test). The “model” mortar instead maintain a stable spread in the first hours and the texture (i.e. shiny spots) becomes more homogeneous (no bumps or color variation) in time.

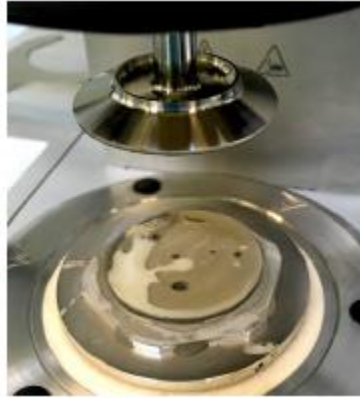


Figure 9: Heterogeneities (i.e. bubbles, sedimentation, migration) shown by one industrial product used for semi-flexible coatings after an oscillation test (plane-plane geometry).

Focusing on our mortar, the temperature of both the bitumen sheet and the cementitious slurry is varied to simulate the real placement conditions. As first, we increased the mortar temperature without varying the bitumen sheet one. The same slurry is tested and the temperature is varied from 25°C to 50°C. To reach this higher temperature we needed a heating time of 1h. Increasing the mortar temperature produces the same effect observed as when increasing time (g. 8 (a)) but in an accelerated way. As an example, a sample heated at 40°C after 30 min, gives a spread of 9 cm which is comparable with the sample shown in fig. 8 (a) after 180 min and at room temperature. Then, we increased the temperature of the bitumen sheet using the same fresh mortar at room temperature. The results are shown in fig. 10.

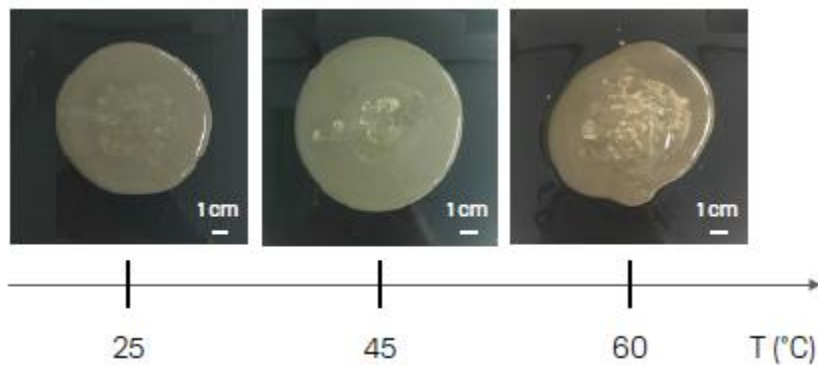


Figure 10: Bitumen sheet temperature effect on the spread of fresh mortar slurry at 25°C.

Once the temperature of the bitumen sheet is raised, the final spread slurry seems more unstable showing an increase of shiny spots in the inner part of the samples, as shown in fig. 10. Moreover, the spread diameters do not differ significantly and at 60°C the bitumen is deformed by the mortar.

Another qualitative way to verify the slurry stability is to produce vibration around the bitumen plate after the slump test. The spread diameter variation is not so high (1.5 cm max) but a “layering” effect is observed for some slurries. In particular, in fig. 11 three samples are showed: (a) fresh mortar at room temperature, (b) fresh mortar on a plate at 60°C, and (c) mortar after one hour at room temperature. The first two samples, after vibration, shown three distinct layers. Qualitatively, starting from the center, there is the less dense layer (shiny spots), then in the successive layer the density increase to be reduced again in the last one. This “layering” phenomenon is not observed in the aged slurry (fig. 11 (c)).

These preliminary slump tests give us an insight about the key parameters

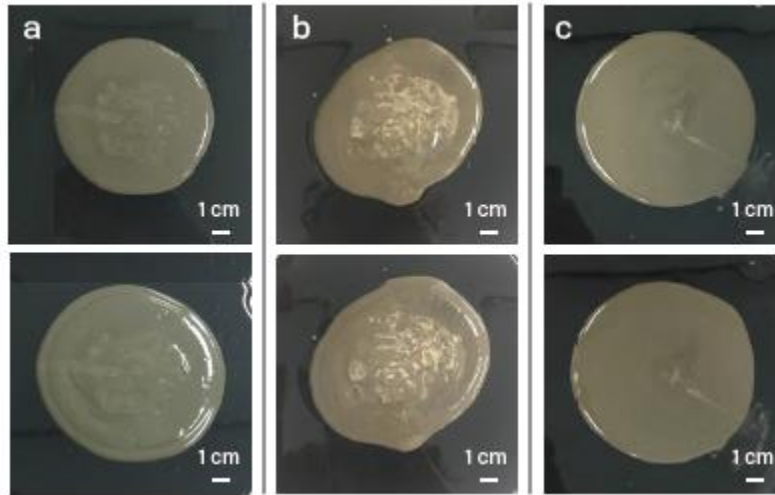


Figure 11: Slurries before and after vibration: (a) fresh mortar at room temperature, (b) fresh mortar on a bitumen plate at 60°C, and (c) mortar after one hour at room temperature.

(i.e. time and temperature) to follow in more details in the next rheological measurements. Further tests on mortar with a higher content of ACE 430 (i.e. 0.4, 0.5 % bwoc) are also planned to obtain a spread similar to the one industrial product.

Moreover, these results allow to have an indirect measure of the slurries yield stress τ_y . The proposed expression for a pure shear flow— so when the horizontal layer of uniform thickness is much smaller than its radial extent $H \ll R$ — is:

$$\tau_y = \frac{225 \rho g \Omega^2}{128 \pi^2 R^5}$$

where Ω is the sample volume, ρ is the material density and R is the spreading radius. Using this equation, the calculated yield stress of our fresh mortar is 9.6 Pa and 6.2 Pa after vibration (fig. 11 a).

This last value is in very good agreement with the preliminary rheological flow test made with a Viskomat NT (Schleibinger), shown in fig. 12 for two different mortar samples (w/c ratio of 0.4 and 0.3% bwoc of ACE 430). These experimental points are fitted with an Herschel-Bulkley model giving an average yield stress of 6.5 Pa.

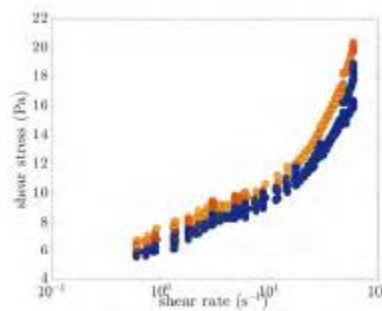


Figure 12: Flow curves for two different mortar samples with a w/c ratio of 0.4 and 0.3% bwoc of ACE 430.

0.4.2 Local rheology: USV

As already mentioned, the Ultrasonic Speckle Velocimetry technique (USV) is coupled to rheometry and was developed at the ENS of Lyon by the Prof. S. Manneville 10 . This innovative and unique apparatus (fig. 13) allows to have at the same time global and local information, correlating rheological measurements with the ultrasonic speckle signal in time.

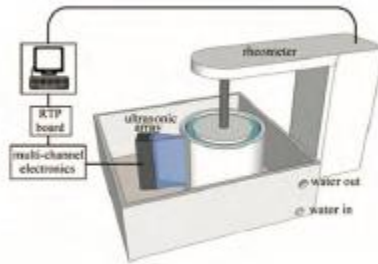


Figure 13: Three-dimensional general view showing the Couette geometry coupled to the ultrasonic device¹⁰.

The local rheology play a fundamental role in the behavior of the slurry during the processing, transport and placement. For this reason, together with the Prof. S. Manneville, we verified the eligibility of this technique on mortar with an exploratory study detailed below.

For these specific measurements Karawanken cement is used with a w/c ratio fixed at 0.3, 1.65% bwoc of ACE 430 and 0.4% bwoc of Sikatard. The global rheology was studied by oscillation and rotation measurements, as shown in fig. 14.

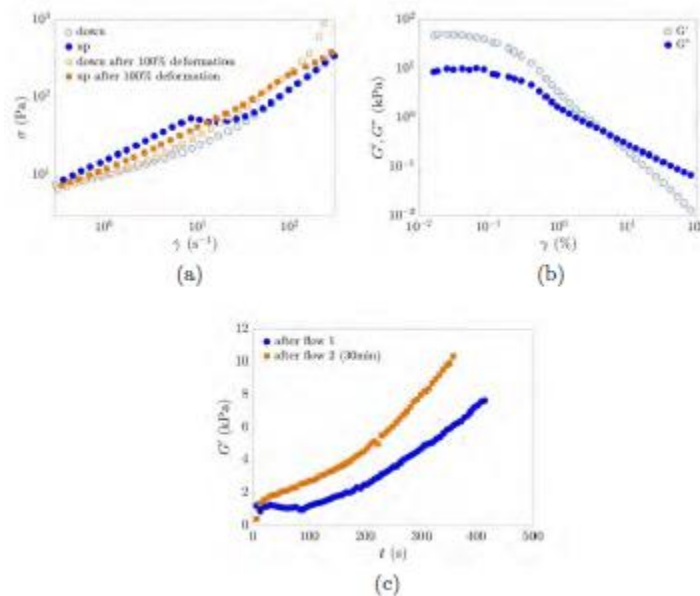


Figure 14: (a) Flow measurements: shear stress σ as a function of the shear rate $\dot{\gamma}$ for the fresh slurry and after 100% of deformation (shown in (b)). (b) Elastic G' and viscous G'' modulus as a function of deformation γ . (c) Elasticity recover in time after the two flow measurements.

In particular in fig. 14 (a) is shown the flow behavior for a fresh sample (blue dots) and after 100% of deformation (orange squares)— test shown in fig. 14 (b). Both flow measurements give a similar trend with an yield stress around 10 Pa. After each flow measurement, the sample underwent a fixed small oscillation to follow the elasticity recover in time (i.e. structural build-up), as shown in fig. 14 (c). Here, the orange line is higher than the blue one because of the sample aging (i.e. setting). From fig. 14 (b) we can also define the elastic domain of our sample (i.e. from solid to liquid behavior). In particular, the elastic modulus G' for small deformation— which is around 50 kPa—and the critical strain around 0.1%.

The most interesting part, and unique ability of the USV setup, is to couple this global information with the local velocity profile. Figure 15 shows velocity profiles acquired at three different shear rate: 100, 50 and 5 s⁻¹. These three shear rate points can be associate with the flow behavior of fig. 14 (a).

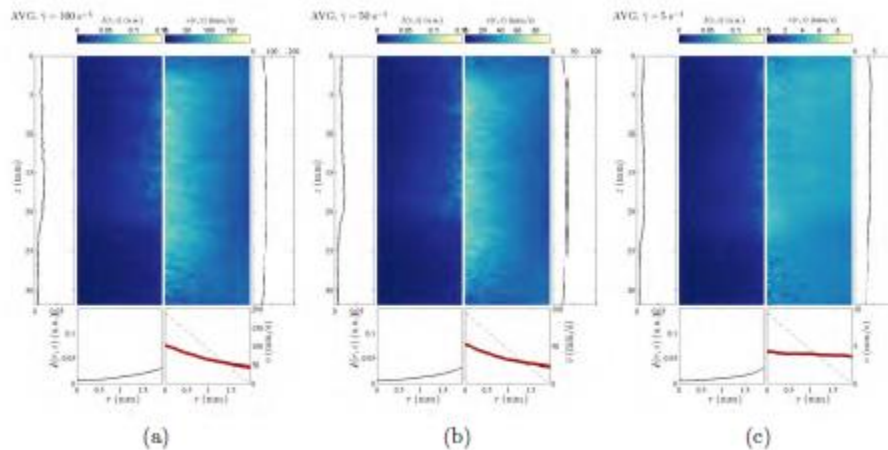


Figure 15: Velocity and intensity profiles along z and r directions for $\dot{\gamma}$ to equal 100, 50 and 5 s^{-1} .

As sketched in the red rectangle of fig. 6, the USV follow the sample along the geometry gap ($r=2$ mm) and through the vertical direction ($z=30$ mm). Figure 15 shows in fact both the intensity and the velocity profiles along the z (vertical) direction and through the gap r .

In particular, the analysis of the two speckles gives information about the homogeneity of the sample and its velocity in the vertical direction (i.e. sedimentation, migration...). We can see that our sample is not completely homogeneous along z , especially at high shear rate (fig. 15 (a)).

Focusing on the velocity profile along the gap (in red) we can observe that the sample presents wall slip at both the rotor (left, $r=0$ mm) and the stator (right, $r=2$ mm). In fact, the red dots do not match the black dotted lines which represent the flow of an ideal fluid. Moreover the slurry is mostly stopped at low shear rate (fig. 15 (c)).

These preliminary tests show the importance of checking the local velocity profiles to avoid erroneous conclusions on the rheology of a mortar. Here, we could verify the eligibility of the technique and concluded on the necessity to make further tests to define the properties of mortars for specific applications.

0.5 Perspectives

The experiences detailed in this report allow to trace the future path of this research. As already mentioned, the next infiltration setup will be built in plexiglass instead of glass and micro-indentation tests will be investigated to characterize the final sample (after setting and cutting).

In a second step, thanks to a collaboration with Prof. Hofko at the TU department of Road Research, we are planning to test mortar infiltration in real porous asphalt samples. Moreover, the results obtained by slump tests on bitumen sheets will be further investigated by rheological measurements (both global and local) in order to quantify the stability and homogeneity of mortars. In particular a collaboration with Prof. Manneville is already planned at the ENS of Lyon.

References

- [1] Q. L. Loh and C. Choong, *Tissue Engineering Part B: Reviews*, 2013, 19, 485–502.
- [2] H. Okamura and M. Ouchi, *Journal of advanced concrete technology*, 2003, 1, 5–15.
- [3] J. A. Bogas, A. Gomes and M. Pereira, *Construction and Building Materials*, 2012, 35, 1013–1022.
- [4] A. A. Busari, J. O. Akinmusuru, B. I. O. Dahunsi, A. S. Ogbiye and J. O. Okeniyi, *Energy Procedia*, 2017, 119, 863–869.
- [5] M. Nepomuceno, L. Oliveira and S. M. R. Lopes, *Construction and Building Materials*, 2012, 26, 317–326.
- [6] B. Bijker-Simsir and L. Rainer, *The Getty Conservation Institute*, Los Angeles, 2013.
- [7] Z. Tan, S. A. Bernal and J. L. Provis, *Materials and Structures*, 2017, 50, 235.
- [8] J. Zhang, J. Cai, J. Pei, R. Li and X. Chen, *Construction and Building Materials*, 2016, 115, 582–592.
- [9] N. Roussel and P. Coussot, *Journal of rheology*, 2005, 49, 705–718.
- [10] T. Gallot, C. Perge, V. Grenard, M.-A. Fardin, N. Taberlet and S. Manneville, *Review of Scientific Instruments*, 2013, 84, 045107.

[11] T. Liberto, M. Le Merrer, C. Barentin, M. Bellotto and J. Colombani, *Soft Matter*, 2017, 13, 2014–2023.

WP 4: Investigation of the influence of the mixing process

Lab mixers were purchased to mix smaller batches with good reproducibly. Protocols were established. A precise rheometer was purchased to be able to make quantitative measurements on cements, but the campaign has not started yet (lab move from Aspanggründe to Arsenal).

WP 5: Influence of cement grain size distribution on concrete rheology, foamability and setting properties

The influence of surfactant nature on the foamability of solution with various concentrations of calcium ions was investigated. All surfactants reduce their ability to form foam with increasing calcium ion concentrations.

Limestone powder, with an average size of 2 μm , has shown to improve the stability of the foam.

This work package is fully detailed in the global report: A3 "Production of thermal insulation material with low density foamed concrete "

Zusammenfassung:

Im vorliegenden Berichtszeitraum wurde nach der Definition von Subsystemen (Wechselwirkung der einzelnen Phasen), schwerpunktmäßig der Fragestellung nachgegangen, wie oberflächenaktive Substanzen in Bezug auf ihre Verschäumbarkeit und Stabilität bei zunehmender Calciumionenkonzentration und Alkalinität beeinflusst werden. Es ist interessant zu beobachten, dass die untersuchten oberflächenaktiven Substanzen ihr Vermögen Schaum zu bilden, mit steigender Calciumionenkonzentration vermindern. Die ethoxylierten Tenside wie Hoesch T9 und Hoesch T12 haben in einer entmineralisierten Lösung die höchsten Verschäumungszahlen, welche aber auch bei hohen Calciumionenkonzentrationen am stärksten zurückgehen. Anders sieht es bei der Filmzerfallszeit aus. Hier kommt es bei fast allen oberflächenaktiven Stoffen bei Anwesenheit von Calciumionen zu einer leichten Stabilisierung.

Die in 3.2.1 beschriebene Methode (Verschäumung mittels schnelllaufenden Rührwerkzeugen) eignet sich sehr gut um schnelle und reproduzierbare Daten zur Verschäumbarkeit der oberflächenaktiven Substanzen zu erhalten. Sie liefert jedoch nur die maximale Verschäumbarkeit der Stoffe unter den definierten Rahmenbedingungen. Für weitergehende Untersuchungen mit dem Fokus auf die Abhängigkeiten zwischen Dichte, Porosität und Viskosität der wässrigen Schäume soll eine maschinelle Verschäumung mittels statischen Linearmischers (Schaumgenerator) wie in 3.2.2 beschrieben verwendet werden. Durch diese Methode lassen sich gezielt unterschiedliche Dichten bzw. Porositäten von wässrigen Schäumen produzieren, die in weiterer Folge Erkenntnisse zur Stabilität sowie rheologischen Eigenschaften des Schaums führen sollen. Die Beeinflussung der Fließgrenze ist hinsichtlich der Fragestellung einer vertikalen Applikation relevant (Fließgrenze > hydrostatischer Druck).

Die angewandte Methode zur Filmstabilitätsuntersuchung wie in 3.3.1 beschrieben, ist primär für Trenduntersuchungen geeignet. Umwelteinflüsse wie bspw. Zugluft und der Faktor Mensch führen zu teils sehr großen Streuungen. Daher muss das Messverfahren weiter verfeinert werden um signifikante Daten zu erhalten. Wie in den Ergebnissen ersichtlich, lässt sich mit Ausnahme von SDS, bei allen oberflächenaktiven Stoffen eine leichte Stabilisierung des Films durch höhere Calciumionenkonzentration feststellen. Wie aus der Literatur bekannt, lässt sich die Stabilität der wässrigen Schäume durch Partikel und Chemische Verbindungen weiter erhöhen. Erste Vorversuche mit fein gemahlene Kalksteinmehl bzw. Additivbeigabe wie Zellulosederivate und (Poly-)Alkohole bestätigen dies. Siehe 4.1.10. Die bisherigen Stabilitätsuntersuchungen betrachten als erste Annäherung einen 2-dimensionalen vertikalen Tensidfilm. Um weitere Erkenntnisse über Schaumstabilität zu erhalten, werden die Versuche um die in 3.3 beschriebenen Methoden ergänzt.

Aufgrund der thermodynamischen Instabilität von wässrigen Schäumen ist in Hinblick auf die Produktion von Betonschäumen eine schnelle Abbindung des Zements von hoher Bedeutung. Weiterführende Untersuchungen sollen einen Eindruck über die Abbindeverzögerung durch die oberflächenaktiven Substanzen geben. Es ist anzunehmen, dass diese Verzögerung bei diversen Schaummitteln unterschiedlich hoch ausfällt.

WP 6: Interfaces between old material and new concrete

1. Zielsetzung

Ziel ist die Charakterisierung von verschiedenen vorbereiteten Betonoberflächen mittels stereoskopischem Verfahren, Sandfleckmethode, Keilspaltmethode und anderen mechanischen Untersuchungen. Die Kenntnisse über die Oberflächenbeschaffenheit des Untergrundes ist essenziell, da die Verbundwirkung zwischen dem Untergrund und des Aufbetons von der Interaktion der beiden Schichten abhängig ist. Um ein günstiges Verbundverhalten zu erzielen, wurden geeignete Vorbereitungs- verfahren, wie das Kugelstrahlen, sowie das Applizieren unterschiedlicher Haftbrücken untersucht.

2. Versuche

Zur Charakterisierung von verschiedenen vorbereiteten Oberflächen wurden ausgewählte Versuche mithilfe von stereoskopischen Untersuchungen, direkten quantitativen topografischen Messverfahren wie die Sandflächenmethode sowie mithilfe von mechanischen Untersuchungen durchgeführt. Tabelle 1 zeigt eine Zusammenstellung der Probekörper sowie deren Oberflächenbearbeitung bzw. die aufgetragenen Haftbrücken. Die Probekörper P3 und P4 sind jeweils zweifach vorhanden (P31, P32/P41, P42) und weisen identische Eigenschaften auf, wobei jeweils einer von diesen Probekörpern (P31 und P41) stereoskopisch untersucht wurde. Bei dem zweiten, identen Probekörper wurden jeweils durch Applizieren einer Haftbrücke mit anschließendem Einbau des Aufbetons mechanische sowie bruchmechanische Untersuchungen durchgeführt. Weiters handelt es sich bei den später mit P5, P6 und P7 bezeichneten Probekörpern um hochdruckwassergestrahlte Oberflächen, die mit unterschiedlichen Intensitäten bestrahlt wurden. Die Ergebnisse dieser Probekörper wurden aus der Dissertation „Bruchmechanische und stereoskopische Charakterisierung von Interfaces zementgebundener Werkstoffe“ von Herrn Martin Peyerl aus dem Jahr 2012 entnommen, um einen breiteren Vergleich der Oberflächen- bearbeitungsmaßnahmen zu erhalten.

Probekörperbezeichnung	Oberflächenbearbeitung bzw. Oberflächenbeschaffenheit
P1	Geschalte Oberfläche
P2	Abgezogene Oberfläche
P3 ₁	Einmal Kugelstrahlen
P3 ₂	Einmal Kugelstrahlen und Epoxidharz-Haftbrücke
P4 ₁	Zweimal Kugelstrahlen
P4 ₂	Zweimal Kugelstrahlen und zementgebundene Haftbrücke

Tab. 1: Zusammenstellung der Probekörper

Die Oberflächenvorbereitung erfolgte durch Kugelstrahlen (siehe Abb. 1).



Abb. 1: Vorbereitung für Kugelstrahlen (links), Kugelstrahlen (rechts)

2.1 Stereoskopische Charakterisierung der Oberflächen

Die Ermittlung von Oberflächenparametern wurden mittels dem stereoskopischen Verfahren und der verwendeten Software MeX durchgeführt. Um eine dreidimensionale Visualisierung der Oberflächen zu ermöglichen und zur Bestimmung von Oberflächenparametern, erfolgte die Aufnahme von zwei um wenige

Grad verkippten Fotos mit einer Spiegelreflexkamera. Für die Fixierung sowie zur richtigen Positionierung der Kamera wurde vorerst ein Gestell in Form eines Rahmens mittels Alu-Steckprofilen gebaut.



Abb. 2: Versuchskonfiguration des stereoskopischen Verfahrens

Die Abbildung 2 zeigt den Messrahmen, mit dessen Hilfe die Kamera zwei um wenige Grad verkippte Fotos aufnehmen kann. Abbildung 3 zeigt beispielhaft die digitalisierte Oberfläche.

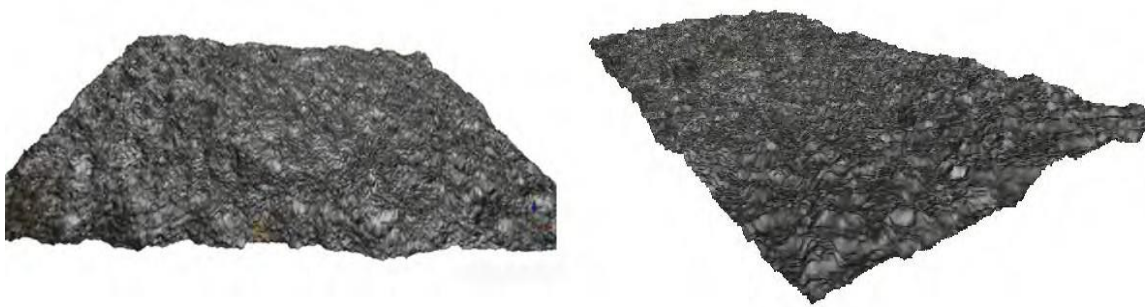
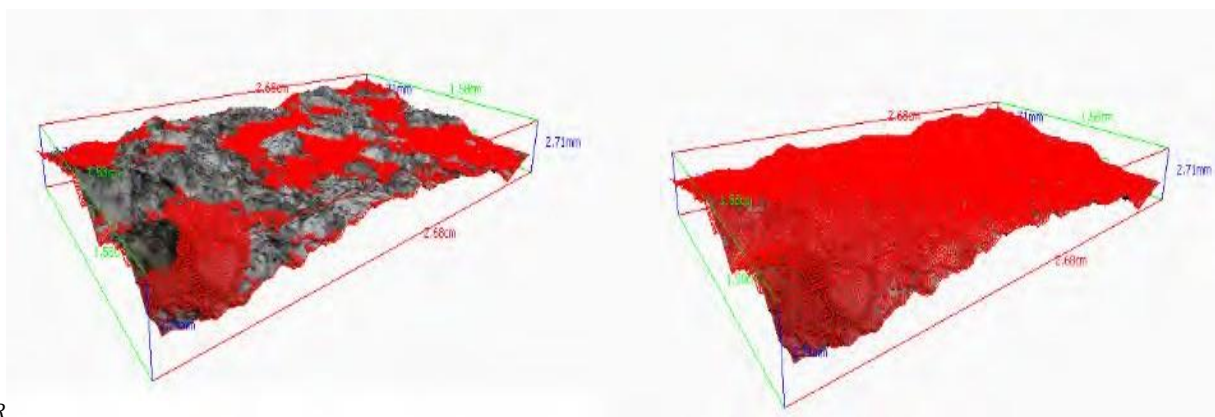


Abb. 3: Darstellung eines digitalen Oberflächenmodells

Die Volumenmessung (Abb. 4) liefert zur Charakterisierung von Oberflächen Parameter wie das Volumen V (unter- und oberhalb der definierten Schnittebene) bzw. die Modi sowie die entsprechende projizierte Fläche A_p . Somit besteht die Möglichkeit, Rückschlüsse auf die Rauheit R_t mithilfe des dreidimensionalen Oberflächenmodells gemäß Gl. 3.1 zu ziehen.¹



R

Abb. 4: Darstellung eines digitalen Oberflächenmodells bei Volumenmessung

¹ Peyerl, Martin: Bruchmechanische und stereoskopische Charakterisierung von Interfaces zementgebundener Werkstoffe. Wien: Technische Universität, Fakultät für Bauingenieurwesen. Diss. 2012. S. 54 – 61.

2.2 Sandflächenverfahren

Zur Ermittlung der Rautiefe R_t wurde 25 ml getrockneter Quarzsand mit einer Korngröße von 0,05 mm – 0,1 mm verwendet. Das feinkörnige Material wurde auf die Oberfläche kegelförmig aufgeschüttet und mit der Rückseite des Sandbehälters (Durchmesser ca. 4 cm) durch rotierende und kreisförmige Bewegungen verteilt und in die Vertiefungen gefüllt (Abb. 51). Abschließend wurde der Durchmesser des Sandflecks an mehreren Stellen gemessen und der mittlere Ellipsendurchmesser berechnet.

2.3 Mechanische Untersuchungen

Probenherstellung

Auf die kugelgestrahlten Oberflächen wurden eine zementgebundene Haftbrücke und eine Epoxidharzhaftbrücke (beide Fa. Glass) nass in nass aufgetragen. Bei der zementgebundenen Haftbrücke wurde vorgemischt.



Abb.5: Auftragung der Haftbrücken (zementgebundene Haftbrücke links, Epoxidharz-Haftbrücke rechts)

Unverzüglich nach der Applizierung der Haftbrücken (Abb. 5) auf die Oberflächen erfolgte die Einbringung des Aufbetons in die Schalung. Nach vollständiger Befüllung der Schalung wurde anhand eines Rütteltisches der Porenanteil des Betons reduziert.

Haftzugversuche

Die Durchführung der Haftzugversuche zeigt Abb. 6, der Scherversuche Abb. 7.



Abb.6: Versuchsdurchführung mit einem automatischen Haftzugprüfgerät



Abb.7: Durchführung des Scherversuches

Keilspaltversuch

Die bruchmechanische Charakterisierung der Verbundfuge erfolgte anhand der Keilspaltmethode, welche die Bestimmung der Kerb-Spaltzugfestigkeit und der spezifischen Bruchenergie erlaubt. Die Versuchsdurchführung ist in Abb. 8 dargestellt.

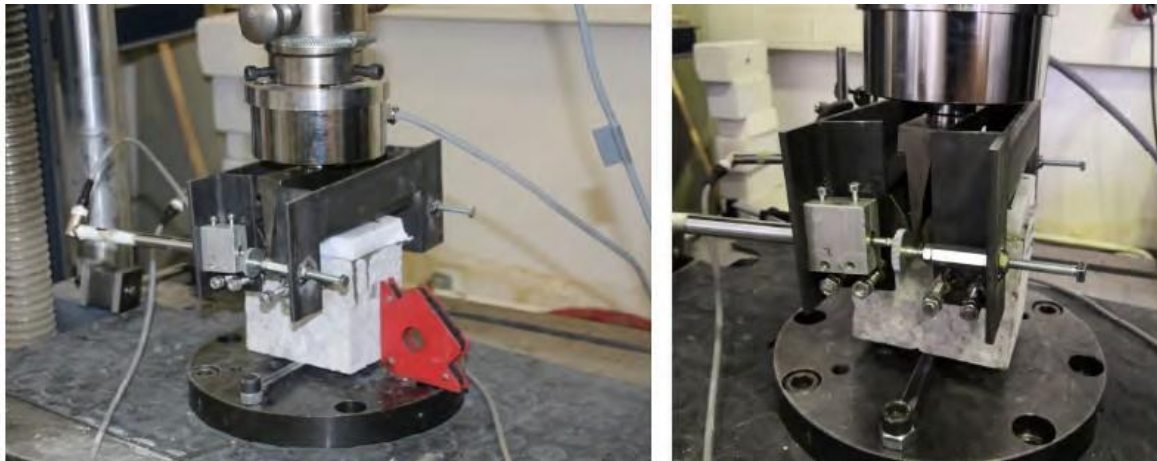
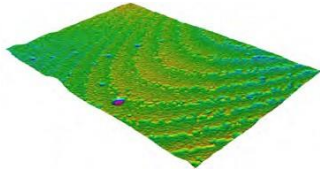
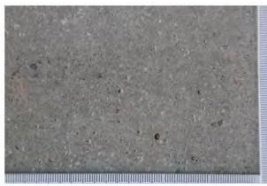
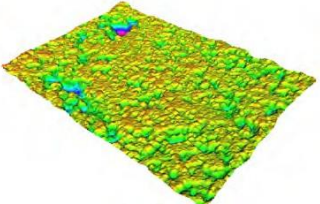

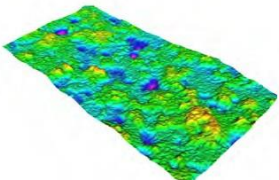
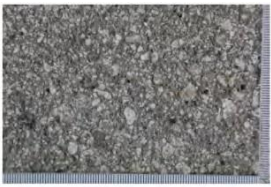
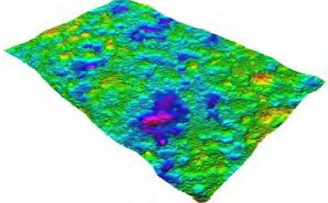



Abb. 8: Versuchseinrichtung sowie Durchführung des Keilspaltversuches

3. Ergebnisse

3.1 Ergebnisse der stereoskopischen Untersuchung

Die Charakterisierung von verschiedenen vorbereiteten Oberflächen wurde vorerst durch die Rautiefenbestimmung mit dem Sandflächenverfahren durchgeführt. Des Weiteren wurde ein dreidimensionales Oberflächenmodell mittels stereoskopischem Verfahren erstellt (Tab. 2) und verschiedenste Parameter wurden ausgewertet. Auf der Grundlage der im Kapitel 3.2 erwähnten Kenngrößen wurden in den folgenden Tabellen die errechneten Parameter der Profil-, Flächen-, und Volumenanalyse für die jeweiligen Probekörper zusammengestellt und verglichen.

Probekörper	Digitales Oberflächenmodell	Oberflächentextur
P1		
P2		
P3 ₁		
P4 ₁		

Tab.2: Dreidimensionale Oberflächenmodelle und die dazugehörige fotografische Aufnahme

Die Werte der Profilanalyse (Tab. 3) zeigen eindeutig, dass die Maximalwerte beim Probekörper P7 und Minimalwerte bei P1 vorlagen. Dies deckt sich mit der Entwicklung der Rauheit R_t , ermittelt durch das Sandflächenverfahren. Ähnliche Zusammenhänge konnten auch bei den Werten der Flächenanalyse (Tab. 4) festgestellt werden. Im letzten Schritt erfolgte die Analyse der Volumenparameter. Dies wurde als wesentlich erachtet, da mithilfe dieses Verfahrens die Bestimmung der Rautiefe mit der Sandfleckmethode simuliert werden kann.

Probekörper- bezeichnung	Parameter der Profilanalyse										
	[mm]										
	Pa	Pq	Pt	Pz	Pmax	Pp	Pv	Pc	Pk	Ppk	Pvk
P1	0,076	0,100	0,685	0,408	0,638	0,234	0,450	0,307	0,222	0,079	0,140
P2	0,126	0,166	0,880	0,657	0,880	0,352	0,527	0,477	0,346	0,079	0,316
p3 ₁	0,246	0,287	1,260	0,848	1,090	0,630	0,625	0,803	0,857	0,164	0,120
p4 ₁	0,259	0,324	1,770	0,861	0,988	0,965	0,807	0,769	0,815	0,356	0,279
P5	0,200	0,260	1,390	0,950	1,380	0,540	0,840	0,720	0,600	0,180	0,380
P6	0,470	0,570	2,620	1,950	2,570	1,100	1,530	1,460	1,170	0,430	0,690
P7	1,160	1,390	5,990	4,030	5,990	3,150	2,840	3,540	3,650	1,180	0,930

Tab. 3: Parameter der Profilanalyse (Minimalwerte fett, Maximalwerte fett und grau hinterlegt)

Probekörper- bezeichnung	Parameter der Flächenanalyse				Parameter der Volumenanalyse	Rautiefe nach Sand- fleckmethode
	[ml/m ²]				[mm]	[mm]
	Vmp	Vmc	Vvc	Vvv	Rto (oben de- ckend)	Rt
P1	14,13	724,62	850,67	55,32	0,120	0,000
P2	49,250	137,587	168,970	125,300	0,270	0,510
P3 ₁	15,760	361,080	4,63,51	36,720	0,280	0,530
P4 ₁	18,820	558,390	671,570	60,360	0,285	0,670
P5	8,980	349,410	389,180	64,130	0,460	0,550
P6	18,270	490,640	596,300	86,870	0,800	0,890
P7	43,770	1543,600	1837,400	232,000	1,970	2,490

Tab. 4: Parameter der Flächen- sowie Volumenanalyse und der Rautiefe nach der Sandfleckme- thode (Minimalwerte fett, Maximalwerte fett und grau hinterlegt)

Das Sandflächenverfahren liefert lediglich einen Einzelwert und kann keine zutreffenden Aussagen über den Zusammenhang mit den Parametern der Profil- und Flächenanalyse liefern. Aufgrund der Ähnlichkeit des Parameters (Rto, oben deckend) aus der Volumenanalyse besteht die Möglichkeit, diese als Vergleichswerte heran- zuziehen und einander gegenüberzustellen (Abb. 9). Auf Basis der in der Tab. 4 dargestellten Parameter Rto und Rt zeigen die folgenden Grafiken einen guten Zusammenhang bzw. eine gute Relation zwischen der aus dem DOM berechneten Rautiefe Rto und der aus dem Sandflächenverfahren ermittelten Rautiefe Rt, da sie nahezu die gleiche Ansteigung verfolgen. Des Weiteren steigt die Rautiefe Rt mit der Anzahl des Kugelstrahlenvorgangs (P31 und P41) sowie mit der Intensität beim Hochdruckwasserstrahlen und erreicht ein Maximum bei P7.

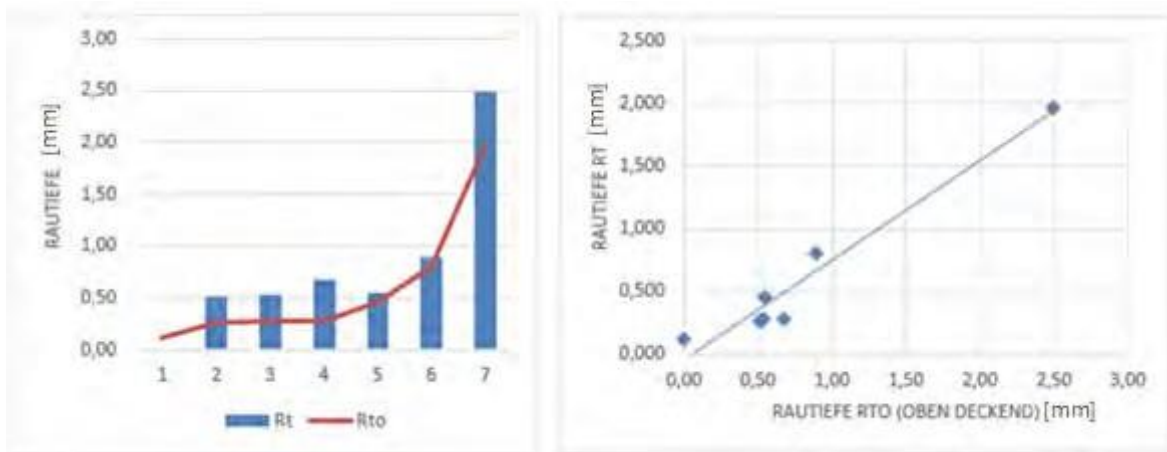


Abb.9: Gegenüberstellung der Rautiefe aus dem DOM Rto und der Rautiefe nach dem Sandflä- chenverfahren

3.2 Ergebnisse der mechanischen Untersuchungen

Druckversuch

Zur Ermittlung von Betoneigenschaften wurde die Druckfestigkeit anhand von zusätzlich drei angefertigten Würfeln mit den Abmessungen 15/15/15 cm bestimmt.

Es ergaben sich folgende Ergebnisse (Tab. 5).

Probe	Masse [g]	Rohdichte [g/m ³]	Bruchkraft [kN]	Druckfestigkeit [N/mm ²]
1	8020	27,07	1052,70	46,79
2	8100	27,34	1011,21	44,94
3	8170	27,57	1010,70	44,92
Mittelwert:				45,55

Tab. 5: Bestimmung der Druckfestigkeit des Betons

Haftzugversuch

Die Ermittlung der mittleren Haftzugfestigkeit erfolgte für die VERbundflächen P32 und P42 jeweils an sechs Probekörpern. Die berechneten Werte sind in der folgen- den Tabelle 6 zusammengestellt.

Haftzugversuch						
Probekörper		Kraft F [N]	Höhe [mm]	Breite [mm]	Fläche A [mm²]	Haftzugfestigkeit σ HZ [N/mm²]
		Epoxidharz-Haftbrücke				
P3 ₂ - 1 x Kugel- strahlen	EP1	3510,0	53,6	53,5	2867,60	1,22
	EP2	3290,0	53,4	53,7	2867,58	1,15
	EP3	3840,0	53,5	55,2	2953,20	1,30
	EP4	3850,0	53,8	56,6	3045,08	1,26
	EP5	3980,0	53,4	51,6	2755,44	1,44
	EP6	5270,0	54,2	51,4	2785,88	1,89
		Mittelwert:				1,38
		Standardabweichung:				0,26
Zementgebundene Haftbrücke						
P4 ₂ - 2 x Kugel- strahlen	ZE1	1970,0	50,2	55,1	2766,02	0,71
	ZE2	2990,0	54,8	55,3	3030,44	0,99
	ZE3	1080,0	50,0	56,5	2825,00	0,38*
	ZE4	3910,0	54,7	56,5	3090,55	1,27
	ZE5	1990,0	54,8	53,2	2915,36	0,68
	ZE6	1620,0	49,7	53,4	2653,98	0,61
		Mittelwert:				0,85
		Standardabweichung:				0,30

Tab. 6: Ergebnisse des Haftzugversuches

Die errechneten Ergebnisse zeigen, dass die höchsten Haftzugfestigkeiten mit einem Durchschnitt von 1,38 N/mm² bei einmal kugelgestrahlten Probekörpern mit Epoxidharz-Haftbrücke (P32) erreicht wurden. Deutlich niedrigere Werte, durchschnittlich 0,77 N/mm², wurden beim zweimal kugelgestrahlten Probekörper mit zementgebundener Haftbrücke (P42) ermittelt. Die Abb. 10 veranschaulicht, dass es bei allen Versuchen zu einem Adhäsionsversagen in der Verbundfuge gekommen ist.



Abb 10: Weitere Bruchflächen Probekörper P42 (Adhäsionsversagen)

Scherversuch

Die durchschnittliche Scherfestigkeit wurde im Rahmen der durchgeführten Untersuchungen anhand von sechs Einzelbestimmungen für den Probekörper P32 und fünf Einzelbestimmungen für den Probekörper P42 ermittelt. Die folgende Tabelle (Tab. 7) veranschaulicht die Ergebnisse der Einzelbestimmungen sowie die Mittelwerte der Scherfestigkeiten. Der Vergleich der Mittelwerte zeigt, dass bei einmal kugelgestrahlten Probekörpern mit Epoxidharz-Haftbrücke (P32) mit durchschnittlichen 1,10 N/mm² etwas höhere Festigkeiten als bei zweimal kugelgestrahlten Probekörpern mit zementgebundener Haftbrücke (P42) mit 0,79 N/mm² erzielt werden konnten. Aufgrund der großen Streuung der Einzelwerte (von 0,32 N/mm² bis zu 2,24 N/mm²) bei beiden Probekörpern ist eine aussagekräftige Beurteilung der Ergebnisse nicht möglich. Tendenziell zeigt die Epoxidharz-Haftbrücke größere Werte.

Scherversuch							
Probekörper		Kraft F [N]	Höhe [mm]	Breite [mm]	Fläche A [mm ²]	Scherfestigkeit σ_S [N/mm ²]	
		Epoxidharz-Haftbrücke					
P3₂ - 1 x Kugelstrahlen	EP1	3194,5	50,7	81,7	4142,19	0,77	
	EP2	2053,0	91,1	70,3	6404,33	0,32	
	EP3	5224,0	91,3	80,6	7358,78	0,71	
	EP4	8500,0	48,0	78,9	3787,20	2,24	
	EP5	6000,0	50,4	81,5	4107,60	1,46	
	EP6	4000,0	51,2	70,1	3589,12	1,11	
		Mittelwert:					1,10
		Standardabweichung:					0,67
		Zementgebundene Haftbrücke					
P4₂ - 2 x Kugelstrahlen	ZE1	9287,0	100,0	81,5	8151,63	1,14	
	ZE3	4142,5	99,1	81,2	8046,92	0,51	
	ZE4	2616,0	100,5	79,1	7949,55	0,33	
	ZE5	7499,0	100,0	81,0	8100,00	0,93	
	ZE6	8298,0	100,0	81,5	8150,82	1,02	
		Mittelwert:					0,79
		Standardabweichung:					0,34

Tab. 7: Ergebnisse des Scherversuches

Die Abb. 11 stellt zum einen die charakteristische Rissbildung in der Verbundfuge dar und zum anderen die jeweiligen Bruchflächen dar.



Abb. 11: Rissbildung in der Verbundfuge und Bruchflächen

Tabelle 8 zeigte die Ergebnisse der Keilspaltversuche

Probekörper	Fm [N]	fFh [m ²]	hlig [mm]	blig [mm]	a [mm]	b [mm]	Alig [mm ²]	Mb [Nmm]	Fh max [N]	Wy [mm ²]	σ [N/mm ²]	KZ	G [J/m ²]
Epoxidharz-Haftbrücke													
P3, - 1 x Kugelstrahlen	EP1	379,8	0,285	80,2	82,3	28,6	40,1	6607	95027	1382,7	88368	1,28	43,14
	EP2	377,7	0,326	81,0	79,2	28,9	40,5	6423	95450	1375,1	86746	1,31	50,75
	EP3	467,9	0,233	81,2	81,5	28,7	40,6	6621	118091	1703,5	89671	1,57	35,19
	EP4	472,4	0,154	81,3	81,1	31,4	40,6	6599	123931	1719,8	89440	1,65	23,34
	EP5	369,2	0,176	80,8	81,9	28,3	40,4	6624	92421	1344,1	89292	1,24	26,57
	EP6	470,1	0,284	80,6	81,5	30,0	40,3	6577	120418	1711,5	88372	1,62	43,18
Mittelwert:											1,45	37,03	
Standardabweichung:											0,18	10,61	
Zementgebundene Haftbrücke													
P4, - 2 x Kugelstrahlen	ZE1	180,1	0,024	81,3	81,4	31,0	40,6	6617	46979	655,7	89671	0,62	3,72
	ZE2	340,3	0,042	80,7	81,4	28,4	40,3	6569	85174	1238,9	88352	1,15	6,42
	ZE3	325,9	0,055	81,0	81,7	24,1	40,5	6620	76664	1186,5	89405	1,04	8,31
	ZE4	383,2	0,051	81,0	80,6	26,4	40,5	6531	93359	1395,1	88223	1,27	7,84
	ZE5	459,3	0,044	80,9	80,8	29,5	40,4	6536	116966	1672,1	88136	1,58	6,87
	ZE6	314,5	0,144	80,6	80,0	29,0	40,3	6448	79427	1145,0	86618	1,09	23,25*
Mittelwert:											1,13	6,63	
Standardabweichung:											0,31	6,97	

Tab. 8: Ergebnisse bzw. Ermittlung der bruchmechanischen Kennwerte

Das linke Diagramm in der Abb. 12 veranschaulicht eine charakteristische Spaltkraft-Verschiebungskurve des Probekörpers P32. Der Verlauf dieser Kurve entspricht annähernd den Einzelbestimmungen von EP1 bis EP6, wobei die maximal erreichbare Horizontalkraft zwischen ca. 1380 N und 1720 N und die maximale Verschiebung zwischen 0,32 mm und 0,70 mm schwankt. Die vorgenommenen Untersuchungen zeigten, dass es beim Probekörper P42 bei allen Einzelbestimmungen – außer ZE6 – beim Erreichen der maximal aufnehmbaren Horizontalkraft und einer sehr kleinen Verschiebung zu sprödem Versagen in Verbundfuge kam. Deshalb ist ein abrupter Verfall der Spaltkraft zu sehen, wobei die Verschiebung konstant bleibt. Das rechte Diagramm entspricht dem typischen Verlauf der Einzelbestimmungen ZE1 bis ZE5. Errechnet wurden maximale Horizontalkräfte von ca. 655 N – 1395 N, wobei die Verschiebung im Gegensatz zu P32 sehr gering ist und zwischen 0,04 mm – 0,08 mm (bei ZE6 0,19 mm) liegt.

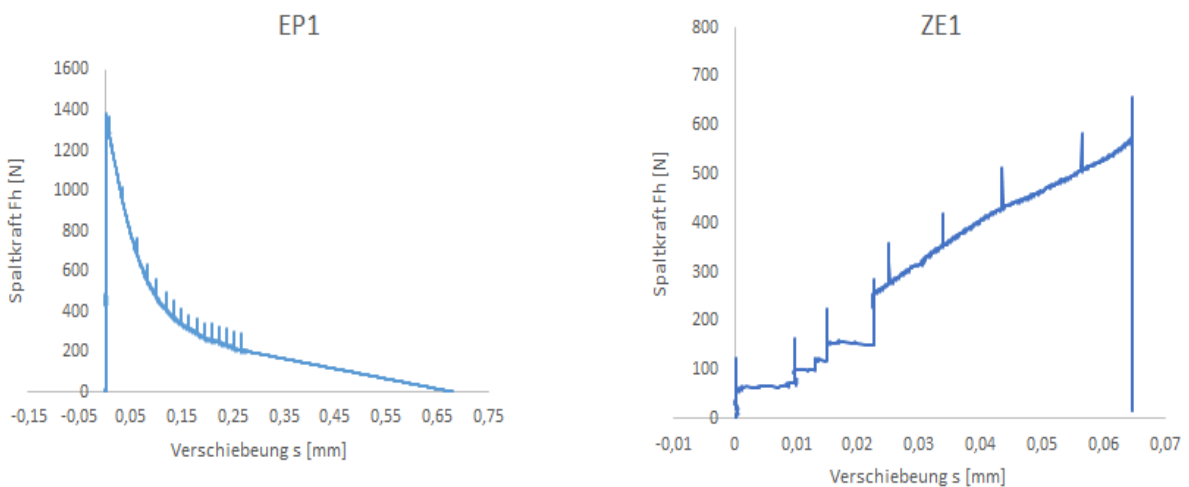


Abb.12: Spaltkraft-Verschiebungsdiagramm, links Probekörper P32, rechts Probekörper P42

Die in der folgenden Abbildung (Abb. 13) dargestellten Bruchflächen weisen Ähnlichkeiten mit allen durchgeführten Einzelmessungen auf.



Abb. 13: Bruchfläche eines Probekörpers mit Epoxidharz-Haftbrücke (links) und eines mit zement- gebundener Haftbrücke (rechts)

4. Resümee

Die durchgeführten Untersuchungen zeigen, dass die Rautiefenbestimmung mit der Sandfleckmethode eine grobe Charakterisierung der Oberfläche mit einem Einzelwert ermöglicht. Mit dem stereoskopischen Verfahren können zahlreiche Parameter zur Charakterisierung der Oberflächentexturen gewonnen werden.

Die Ergebnisse der mechanischen Untersuchungen sind in Abbildung 14 zusammen- gestellt. Es zeigt sich, dass die mechanischen sowie bruchmechanischen Untersuchungen beim Probekörper P32 (Epoxidharz-Haftbrücke) höhere Festigkeiten als beim Probekörper P42 (zementgebundene Haftbrücke) liefern. Es wurde ebenso nachgewiesen, dass die Bestimmung der bruchmechanischen Kennwerte, wie die spezifische Bruchenergie, bei der Charakterisierung von Verbundfugen von großer Bedeutung ist. Denn die größte Abweichung im Gegensatz zur Haftzug-, Scher-, und Kerb-Spaltzugfestigkeit konnte bei der spezifischen Bruchenergie ermittelt werden, und zwar ist diese bei der Epoxidharz-Haftbrücke (P32) ca. fünfmal so groß wie bei der zementgebundenen Haftbrücke (P42).

Zuletzt ist festzuhalten, dass die Verbundfuge, die mit einer Epoxidharz-Haftbrücke versehen ist, deutlich bessere Verbundeigenschaften aufweist als die mit der zement- gebundenen Haftbrücke. Die höheren Werte können auf die spezifischen Eigenschaften der applizierten Haftbrücke zugeführt werden.

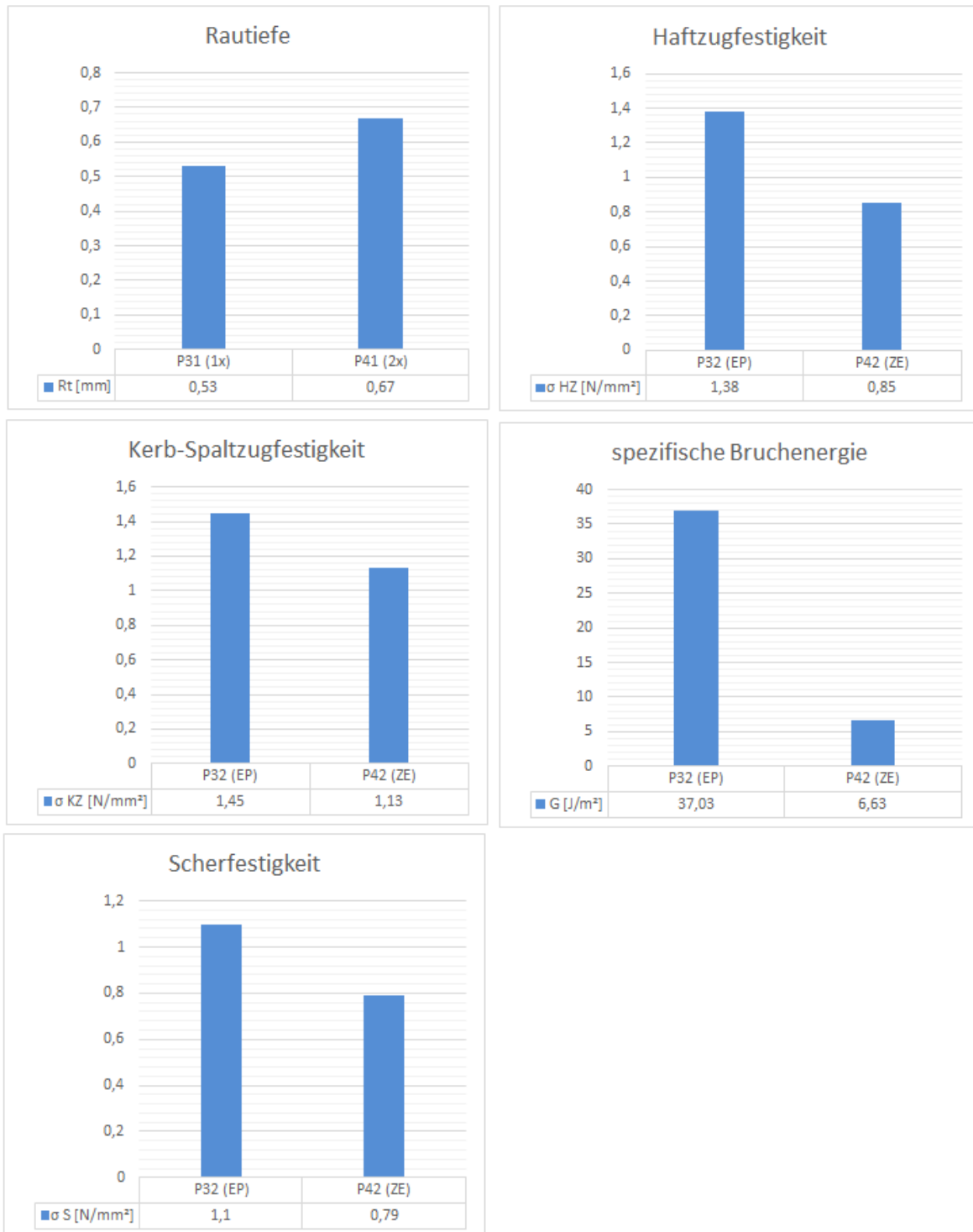


Abb. 14: Ergebnisse der Bestimmung der Rautiefe, der Haftzugfestigkeit, der Kerb-Spaltzugfestigkeit, der spezifischen Bruchenergie und der Scherfestigkeit

WP 7: Device for measuring infiltration

This study on mortar injection in porous media is focused on three main applications: (i) infiltration for semi-rigid coatings, (ii) expanded clay concrete for thermal insulation materials, and (iii) building renovation. In order to make a quantitative study about the slurry penetration and improve the robustness of the product for easier placement, laboratory setups to mimic the mentioned applications are being designed, enabling well controlled experiments.

A home-made setup to mimic infiltration in porous asphalt was first designed. A cylindrical glass geometry filled with glass beads was used and coupled with an optical setup to follow the mortar infiltration in time.

Infiltration setups

One important physical quantity that characterizes a porous medium is its porosity, that in our case need to match the final application properties (i.e. asphalt skeleton). Another important quantity is the permeability, so a measure of the fluid flow in a porous medium under the action of a pressure difference. When the fluid phase is not continuous (i.e. the pores do not communicate with each other), the porous medium is not permeable. We want to verify the medium permeability starting from an ideal system (i.e. glass beads) to extend later the study to real samples (i.e. asphalt samples).

Then, in order to mimic mortar infiltration in porous media, we are investigating three setups inspired by testing procedures classically used in the architectural conservation field. In particular, on the left side of fig. 2, two under gravity setups are sketched to mimic infiltration in asphalt (glass beads) or small fractures (capillaries). On the right side instead is shown an injection grouting for crack repair under pressure.

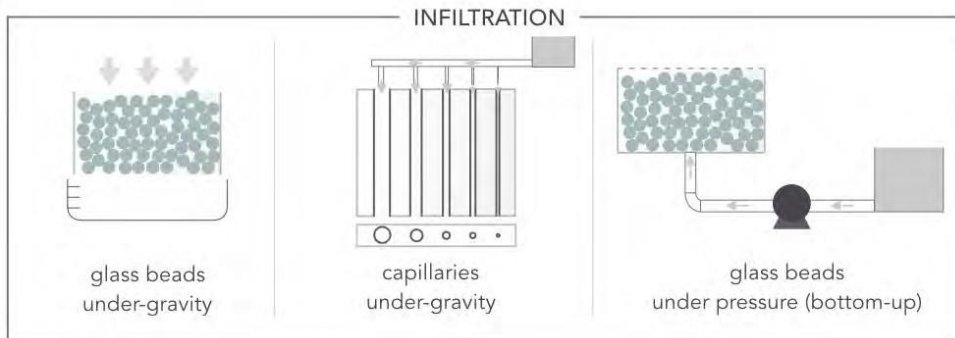


Figure 2: Setups for mortar infiltration tests in porous media.

Glass beads under gravity

A preliminary study consists in having a mortar infiltrated a pack of glass beads under gravity. A cylindrical glass geometry is filled with these beads to mimic the asphalt skeleton from semi rigid coatings (Halbstarre Deckschichten). At this early stage, wettability of the infiltrated medium, shape of particles, and all other complexity related to the real medium is not considered. Following the requirements for semi-rigid surface courses (RVS 08.16.03), the glass beads dimensions are chosen equal to 8, 12, 16 mm. Tests are made on glass filled with mono and poly-disperse glass beads. In particular, we tested mortar flow on cylindrical glasses entirely filled with respectively 8, 12, 16 mm and a combination of the three: 50% of 8 mm, 33% of 12 mm and 17% of 16 mm. After filling the cylinder glass with the beads, the sample is heated at 300° C/h for two hours, kept at 600° C for 30 minutes and after is slowly cooled to 20°C. Then, in the bottom part two symmetric and millimetric holes are made to allow the mortar flush out. To follow the infiltration in time, we used an optical setup with a rapid camera (BASLER piA640-210gm/gc) and a backlight window as shown in fig. 3.



Figure 3: Optical setup for mortar injection in a cylinder filled with glass beads.

In fig. 4, from (a) to (d) we can observe the progressive infiltration of a mortar with a w/c ratio of 0.4 and 0.4%

of ACE 430. In all the tested systems, the infiltration is quite fast (4-5 s), and this time is likely dictated by the size of the bottom hole rather than by the rheological properties of the slurries. The slurries penetrate easily the entire depth of the glass cylinder.

This aspect can be verified by the optical images but also cutting the samples after the mortar setting, as shown in fig. 5.

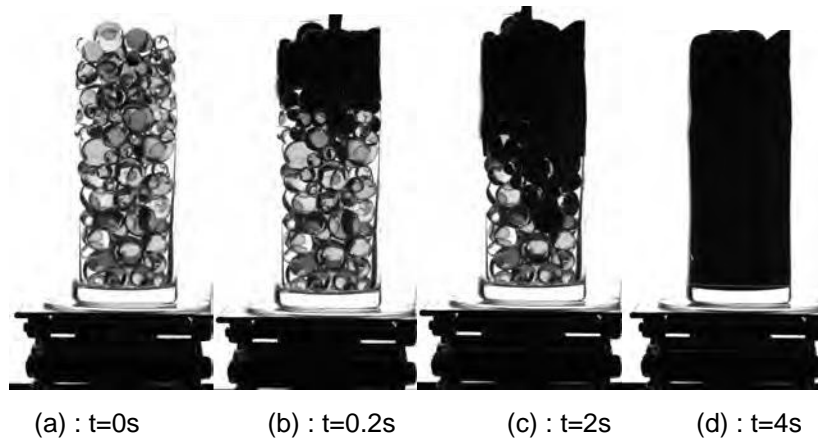


Figure 4: (a)-(d) Images in time of mortar infiltration in the glass beads setup.



Figure 5: Vertical section of the glass cylinder filled with polydisperse glass beads (50% of 8 mm, 33% of 12 mm and 17% of 16 mm) after mortar infiltration and setting.

This cutting operation is difficult to make due to the glass hardness and brittleness. The final section shows several scratches and small fractures and we cannot distinguish if they are result of the setting and glass-mortar interfaces or if they are generated by the cutting operation. Given these experimental difficulties, the next generation setup will use plexiglass instead of glass. Moreover, we will investigate the adequacy of micro-indentation tests to measure the local mechanical properties after setting.

WP 9: Device for characterizing volume changes or limiting pressure of RA concretes

Not started

WP 10: High thermal insulation in a double-walled tower

Not started.

3. Project team and cooperations

- Are there any significant changes in the project team (internal key employees, project team members, project team members) and external partners/third parties)?
- Discuss any changes to the work distribution.

Are there any effects on the cost / financing structure and the objectives?

There were no changes in the project team of the internal key employees.

Organization of the external scientific partner (participation of Mr Deix, Mr Kirnbauer, Mr Lebeda, Mrs Merta, Mr Stöttner) and new recruits (Post-doc Teresa Liberto and PhD student Dana Daneshvar)

Ildiko Merta started 01.01.2019 20H/Woche.

Teresa Liberto started 14.01.2019 40H/Woche

Dana Daneshvar started on 11.09.2019 10H/Woche

There is no impact on the cost / financing structure and objectives.

4. Economic and scientific exploitation

- Describe the previous exploitation and / or redistribution activities. Is recycling possible?
- List publications, dissertations, diploma theses and any patent applications, that emerged from the project.
- What further R&D activities are planned?
- How will the prototypes created in the project be further used?

The investigations regarding interface have been incorporated in the following works:

Untersuchung des Beton-Interfaces für die Instandsetzung von Brückenbauwerken mit Aufbeton

Stereoskopische, mechanische und bruchmechanische Charakterisierung von verschiedenen vorbereiteten Betonoberflächen bei Aufbringung weiterer Betonschichten im Verbund, Masterarbeit von Muhammed Yunus Yildirim, FH Campus Wien, 8.7.2019

Anwendbarkeit von Untersuchungsmethoden zur Charakterisierung der Verbindung zwischen Alt- und Neubeton

Interface Beton, Bachelorarbeit Alban Mehmetaj, 11.7.2019, FH Campus Wien

Furthermore it is planned:

Master thesis Marijan Tomic, FH Campus Wien, Start in Nov. 2019

5. Notes on Costs & Financing

- Billing takes place directly in eCall or via Excel for projects submitted by Sept. 2015. In eCall, the right variant for you is automatically presented to you.
- Please refer to the FFG cost guide (www.ffg.at/kostenleitfaden) and tender documents.
- Deviations from the cost plan must be described and justified at this point.

In the first research year there were no deviations from the cost plan.

6. Project-specific special conditions and requirements

- Address project-specific special conditions and requirements (according to §6 of the grant agreement), if these have been agreed in the grant agreement or contract for work and services.

The project-specific conditions and requirements are met.

7. Reportable events

Are there any special events concerning the funded project which must be reported to the FFG (see also Guidelines - Appendix to 5.3., 5.3.5), e.g.

- Changes in the legal and economic possibilities of influence of the Recipient
- insolvency proceedings
- events which delay the performance of the subsidised service or render impossible
- Further funding for this project

In the first year of research, there were no notifiable events.